npj Precision Oncology

https://doi.org/10.1038/s41698-026-01358-5

Article in Press

NDUFA4L2 regulates the progression and chemotherapy sensitivity of HNSCC by inhibiting PANoptosis

Received: 12 November 2025

Accepted: 23 February 2026

Cite this article as: Cui, J.-J., Yang, Y., Zhao, J.-H. *et al.* NDUFA4L2 regulates the progression and chemotherapy sensitivity of HNSCC by inhibiting PANoptosis. *npj Precis. Onc.* (2026). https://doi.org/10.1038/s41698-026-01358-5

Jing-Jing Cui, Yang Yang, Jia-Hao Zhao, Yu-Jia Guo, Meng-Ran Zhao, Ran Zhao, Yue-Han Li, Jun-Yao Wu & Xiaomeng Song

NDUFA4L2 regulates the progression and chemotherapy sensitivity of HNSCC by inhibiting PANoptosis

Jing-Jing Cui [1,2], Yang Yang [1,2], Jia-Hao Zhao [1,2], Yu-Jia Guo [1,2], Meng-Ran Zhao [1,2], Ran Zhao [1,2], Yue-Han Li[1,2], Jun-Yao Wu[1,2], Xiaomeng Song [1,2, *]

[1] State Key Laboratory Cultivation Base of Research, Prevention and Treatment of Oral Diseases, Jiangsu Province Engineering Research Center of Stomatological Translational Medicine, Nanjing Medical University, Nanjing 210029, China

[2] Department of Oral and Maxillofacial Surgery, The Affiliated Stomatological Hospital, Nanjing Medical University, Nanjing 210029, China

Prof. Xiaomeng Song, School and Hospital of Stomatology, Nanjing Medical University, Nanjing 210029, China. Tel: +86-25-69593120; Fax: +86-25-69593186; E-mail: xiaomengsong@njmu.edu.cn

Abstract

Head and neck squamous cell carcinoma (HNSCC) represents a leading global malignancy among head and neck cancers. While chemotherapy serves as a standard adjuvant treatment, cisplatin resistance frequently compromises therapeutic outcomes. PANoptosis is an integrated inflammatory cell death pathway governed by PANoptosome complexes. It critically influences chemotherapy response, though its regulatory mechanisms remain incompletely characterized. NADH dehydrogenase (ubiquinone) 1 alpha subcomplex subunit 4-like 2 (NDUFA4L2), a subunit of respiratory chain complex I, has been identified as a critical regulator of cell survival. Our multi-platform investigation employed HNSCC cell lines, patient-derived organoids, tongue orthotopic xenograft models in C57BL/6 mice and *Tgfbr1/Pten* 2cKO mice to elucidate the role of NDUFA4L2 in cisplatin resistance. Bioinformatic analysis and clinical samples indicate that elevated NDUFA4L2 is associated with poor survival rates and low sensitivity to chemotherapy in HNSCC patients. Through *in vitro* and *in vivo* studies, we found that NDUFA4L2-KO in combination with cisplatin suppresses glycolysis levels, thereby inhibiting AIM2 inflammasome activation. Consequently, it triggers tumor cell PANoptosis, remodels the immunosuppressive tumor microenvironment, and enhances antitumor efficacy. These findings establish NDUFA4L2 as both a prognostic biomarker and therapeutic target for overcoming cisplatin resistance in HNSCC through PANoptosis modulation.

1. Introduction

Head and neck squamous cell carcinoma (HNSCC) is the seventh most common malignant tumor worldwide, involving the oral cavity, pharynx, hypopharynx, larynx, nasal cavity, and salivary glands[1]. GLOBOCAN estimates indicate that there are 890,000 new cases and 450,000 deaths from HNSCC annually, which account for approximately 4.5% of all cancer diagnoses and deaths[2].Chemotherapy resistance frequently leads to treatment failure when used as an adjuvant treatment for HNSCC[3]. Consequently, identifying targets that inhibit tumor growth and increase chemotherapy sensitivity is essential for enhancing the survival rate and prognosis of patients with HNSCC.

Programmed Cell Death (PCD) is a fundamental process that has evolved in organisms over time to eliminate unnecessary, abnormal, or potentially cancerous cells, thereby maintaining homeostasis[4]. Dysregulation of PCD is closely associated with tumor progression and plays a critical role in cancer treatment, particularly when using cytotoxic drugs that inhibit tumor growth and metastasis by inducing cell death. Among the various forms of PCD, pyroptosis, apoptosis, and necroptosis have been extensively studied[5,6]. PANoptosis is a newly discovered form of regulated cell death that integrates key molecular components of pyroptosis, apoptosis, and necroptosis, simultaneously activating these three death pathways to achieve a synergistic, multimodal killing effect[7]. Importantly, the integrity of biological functions during PANoptosis cannot be simply explained by individual death pathways, and blocking any of these forms of cell death pathways alone is not effective in preventing PANoptsis progression. Furthermore, PANoptsis is characterized by the involvement of multifaceted scaffold compounds, termed the

PANoptosome, which includes proteins such as ZBP1, RIPK1, AIM2, and NLRP12[8,9], and significantly inhibits cancer cell growth and resistance. It also activates a robust anti-tumor immune response and enables tumor-specific induction of PANoptosis as a potential cancer treatment strategy. Currently, only a limited number of studies have demonstrated the correlation between PANoptosis and the development of HNSCC as well as its therapeutic efficacy, while the underlying associations and mechanisms remain insufficiently explored[10,11].

NADH dehydrogenase (ubiquinone) 1 alpha subcomplex subunit 4-like 2 (NDUFA4L2) is a HIF-1α target gene localized in the mitochondria, involved in the composition of the electron transport chain (ETC) complex I subunit and modulating its activity[12]. Previous studies have shown that NDUFA4L2 is upregulated in neoplasms and can inhibit the production of ROS, thereby inducing antioxidative stress in cancer cells[13]. Additionally, NDUFA4L2 overexpression can promote the development of colon adenocarcinoma by activating PI3K/AKT signaling in a ROS-dependent manner[14], while knockdown of NDUFA4L2 can inhibit the viability of non-small cell lung cancer under hypoxic conditions[15]. Moreover, studies in various tumors have displayed that high expression of NDUFA4L2 promotes chemotherapy resistance in tumor cells[16-18]. Currently, it remains unclear how NDUFA4L2 promotes chemotherapy resistance and what its potential roles are in PANoptosis.

In the carcinogenesis process, the genetic alteration of tumor suppressor genes and oncogenes removes the barriers imposed by cells, leading to uncontrolled cell proliferation[19]. To sustain rapid proliferation, cancer cells must adapt metabolically to meet their heightened energetic and biosynthetic requirements—a phenomenon first characterized by Otto Warburg in the 1920s as aerobic glycolysis (the "Warburg effect")[19], wherein glucose is preferentially fermented to lactate even under oxygen-replete conditions. This aerobic glycolysis represents a fundamental metabolic shift in tumor tissues, bypassing mitochondrial oxidative phosphorylation[21]. Recent studies have uncovered that glycolysis related protein and metabolites actively participate in cell death regulation through modulation of apoptotic signaling pathways, revealing novel mechanistic connections between metabolism and cellular demise[22-25]. However, its relationship with PANoptosis has not been thoroughly explored.

This study demonstrates that overexpression of NDUFA4L2 promotes the progression of HNSCC and confers resistance to cisplatin through integrated bioinformatics analysis and experimental validation. Conversely, the absence of NDUFA4L2 enhances the efficacy of cisplatin treatment by inducing AIM2-dependent PANoptosis through the inhibition of glycolysis. Additionally, we have shown that the lactylation level of AIM2 correlates with NDUFA4L2 expression. These findings enhance our understanding of the role of NDUFA4L2 in HNSCC, offer guidance on overcoming the limitations of cisplatin therapy, and assist in the development of effective treatment strategies.

2. Results

2.1. Elevated NDUFA4L2 expression is associated with the development, prognosis, and chemotherapy resistance of HNSCC.

Using non-negative matrix factorization, we identified eight transcriptional modules from

carcinoma in situ datasets (Fig. 1a). UMAP clustering segregated tumor cells into 10 populations, with cluster 4 showing distinct NDUFA4L2 positivity (Fig. 1b, c) and predominant MP6 module expression (Fig. 1d, e; Supplementary Fig. 1, 2). GSEA revealed the association of MP6 module with hypoxia, glycolysis and apoptosis pathways (Fig. 1f). Clinically, elevated NDUFA4L2 correlated with poorer patient survival (Fig. 1g).

Furthermore, we collected samples from six chemotherapy-resistant and six chemotherapy-sensitive patients for Western blot analysis. The results confirmed elevated NDUFA4L2 expression in the resistant cases (Fig. 1h). Besides, Western blot analysis using 5 pairs of matched tumor/normal pairs confirmed the high expression of NDUFA4L2 in tumor tissue (Fig. 1i), while IHC showed a progressive upregulation of NDUFA4L2 from normal tissue to precancerous lesions to HNSCC (Fig. 1j). Consequently, these findings establish that NDUFA4L2 is overexpressed in HNSCC, particularly in treatment-refractory cases. What's more, elevated expression

of NDUFA4L2 is closely linked to tumor hypoxia, glycolysis and apoptosis processes, potentially reducing patient survival. Thus, it is imperative to explore how NDUFA4L2 affects the progression of HNSCC and chemotherapy resistance.

Cell line screening identified CAL27 and FaDu as high NDUFA4L2 expressers (Supplementary Fig. 3), while MOC1 was selected for *in vivo* studies. In three cell lines, NDUFA4L2 was knocked out and verified by Western blot analysis (Supplementary Fig. 4a-c). Cisplatin IC_{50} assays revealed significantly reduced drug resistance in NDUFA4L2-knockdown cells versus controls (Supplementary Fig. 5). Strikingly, applying control-group IC_{50} doses to knockout cells enhanced cytotoxicity (Supplementary Fig. 6), demonstrating the pivotal role of NDUFA4L2 in HNSCC chemoresistance.

2.2. Knockout NDUFA4L2 can trigger PANoptosis in tumor cells and enhance the efficacy of cisplatin.

To evaluate the role of NDUFA4L2 in HNSCC cell behavior, we treated control and NDUFA4L2-KO CAL27, FaDu, and MOC1 cells with cisplatin (IC_{50}). Microscopy revealed enhanced cell death in knockout cells, particularly when combined with cisplatin, with increased pyroptotic blebs[26] versus cisplatin alone (Fig. 2a). Using pathway-specific inhibitors (Z-VAD-FMK for apoptosis, necrostatin-1 for necroptosis, DMLD for pyroptosis)[27-29], we found each inhibitor partially reversed the cytotoxicity of NDUFA4L2-KO plus cisplatin, but none restored viability to control levels (Fig. 2b, Supplementary Fig. 7). These results suggest NDUFA4L2 suppression synergizes with cisplatin to induce multiple forms of cell death.

We generated NDUFA4L2-KO CAL27, FaDu, and MOC1 cells and assessed PANoptosis markers after cisplatin treatment. Regarding apoptosis, Western blots indicated elevated levels of Cleaved Caspase-3/8 in the KO+cisplatin groups (Fig. 2c-e). Furthermore, there was a marked increase in the phosphorylation of mixed lineage kinase domain-like (p-MLKL), a critical initiator of necroptosis (Fig. 2c-e). For pyroptosis, we observed enhanced GSDME cleavage, which is the primary executor responsible for forming membrane pores under specific conditions[30], facilitated by Caspase-3 activation[31] (Fig. 2c-e), consistent with our microscopy findings (Fig.

2a, b). Moreover, we performed Western blot analysis for common core components of the PANoptosome, including ZBP1, NLRP3, and AIM2. We found that NDUFA4L2-KO could plus cisplatin upregulated AIM2 expression, without significantly altering ZBP1 or NLRP3 levels. (Fig. 2c-e).

Besides, we established patient-derived HNSCC organoids (Fig. 2f, g). NDUFA4L2-KO slowed organoid growth, with combination treatment showing enhanced shrinkage versus cisplatin alone (Supplementary Fig. 4d, Fig. 2h). Western blots revealed consistent PANoptosis marker patterns between cells and organoids (Fig. 2i).

These results suggest that the combination of NDUFA4L2 inhibition and cisplatin treatment exerts a synergistic effect across cell lines and organoids, leading to PANoptosis, which includes apoptosis, necrosis, and pyroptosis. This leads us to speculate that NDUFA4L2 may be a broad target for enhancing cisplatin chemotherapy sensitivity.

To assess the function of NDUFA4L2 in tumor growth and chemotherapy response, we established orthotopic tongue tumors in C57BL/6 mice using NDUFA4L2-KO MOC1 cells, followed by PBS or cisplatin treatment (Fig. 3a). NDUFA4L2-KO plus cisplatin significantly inhibited tumor growth and the decrease in mouse body weight (Fig. 3c, e, f), while improving 30-day survival (Fig. 3d). Tumor samples were subjected to Flow cytometry (Fig. 3h-k) and IHC (Fig. 3g), revealing that NDUFA4L2-KO reduced the content of M2 macrophages in the tumor while increasing the content of $CD8^+$ T cells. Western blots confirmed enhanced PANoptosis marker activation (Fig. 3b), mirroring *in vitro* results and demonstrating synergistic therapeutic efficacy. In summary, the above results further highlight the synergistic effect of NDUFA4L2 deficiency and cisplatin treatment *in vivo*.

2.3. Glycolysis is essential for PANoptosis induced by NDUFA4L2 deficiency under cisplatin treatment.

To investigate the role of NDUFA4L2 in cisplatin-induced PANoptosis in HNSCC, we performed RNA-seq on NDUFA4L2-KO and control FaDu cells. NDUFA4L2-KO downregulated glycolysis/lactate metabolism genes (Fig. 4a). Consequently, we measured the lactate levels in CAL27 and FaDu cells. In comparison with the control group, the lactate levels in the NDUFA4L2-KO group were significantly reduced (Fig. 4b).

To test whether glycolysis inhibition triggers PANoptosis via AIM2 activation, we treated CAL27, FaDu, MOC1 cells and organoids with glycolysis inhibitor 2-DG (IC_{50}) ± cisplatin(Supplementary Fig. 8). Microscopy showed pyroptotic blebs similar to NDUFA4L2-KO cells (Fig. 4c), with enhanced organoid shrinkage in combination treatment (Fig. 4d). Western blot confirmed stronger activation of PANoptosis markers (Cle-Caspase-3/8, p-MLKL, GSDME, AIM2) with 2-DG treatment (Fig. e-h), demonstrating glycolysis inhibition promotes PANoptosis.

To validate the antitumor effects of glycolysis inhibition *in vivo*, we performed orthotopic tongue xenografts using MOC1 cells, treating mice with PBS, 2-DG, or cisplatin (Fig. 5a). The 2-DG/cisplatin combination significantly reduced tumor growth (Fig. 5c, d) while attenuating body-weight loss (Fig. 5e) and improving 30-day survival (Fig. 5f), demonstrating enhanced chemotherapeutic efficacy. Flow cytometry and IHC (Fig. 5g) revealed decreased M2

macrophages and increased $CD8^+$ T cells (Fig. 5h-k), indicating improved tumor immunity. Western blots confirmed enhanced PANoptosis marker activation (Fig. 5b). In *Tgfbr1/Pten* 2cKO HNSCC mice (Fig. 6a), H&E/IHC analysis showed delayed tumor progression and improved microenvironment (Fig. 6b, Supplementary Fig. 9), with Western blots corroborating previous findings (Fig. 6c). These results demonstrate that NDUFA4L2 deficiency plus cisplatin inhibits glycolysis to induce PANoptosis.

2.4. NDUFA4L2-KO promotes tumor cell PANoptosis by inhibiting AIM2 lactylation.

Chemoresistance remains a major obstacle in cancer treatment, with resistant tumors often developing immunosuppressive microenvironments. Multiplex immunohistochemistry (mIHC) of six matched chemotherapy-sensitive and -resistant samples revealed significant differences in immune cell infiltration and metabolic markers. Quantitative analysis demonstrated higher $CD68^+CD206^+$ cell proportions, elevated MFI of NDUFA4L2 and Kla, but reduced $CD8^+$ and $CD20^+$ populations in resistant cases (Fig. 6d-i), confirming our prior findings.

To elucidate the role of NDUFA4L2 in PANoptosis regulation, we built upon Western blot data showing NDUFA4L2-KO upregulates AIM2 protein. To investigate whether NDUFA4L2-KO promotes PANoptosis via AIM2 PANoptosome activation, we performed co-IP assays in cisplatin-treated wild-type and NDUFA4L2-KO CAL27 and MOC1 cells. The NDUFA4L2-KO/cisplatin combination enhanced AIM2-ASC interaction and their binding to CASPASE-8 and RIPK1. This group also showed elevated PANoptosis markers (p-MLKL, GSDME-N, Cle-CASP-3/8), confirming AIM2 PANoptosome-mediated PANoptosis induction (Fig. 6j).

Subsequently, we knocked down AIM2 in NDUFA4L2-KO CAL27 and MOC1 cells. Then, we treated them with cisplatin, and analyzed PANoptosis markers and cell viability. Western blot showed AIM2 knockdown attenuated the PANoptosis marker activation caused by NDUFA4L2 knockout plus cisplatin (Fig. 6k). Both Live/dead assays and CCK8 assays demonstrated significantly reduced cytotoxicity from the combination treatment upon AIM2 knockdown(Supplementary Fig. 10, 11), confirming the essential role of AIM2 in this PANoptosis pathway.

However, RT-qPCR analysis in CAL27 and FaDu cells revealed no change in AIM2 mRNA levels following knockout (Fig. 6l), indicating that NDUFA4L2 knockout can increase AIM2 protein abundance without affecting its mRNA level. This suggests that NDUFA4L2 may influence AIM2 protein levels at a post-transcriptional level. Co-IP assays excluded direct NDUFA4L2-AIM2 interaction (Fig. 6m).

Notably, NDUFA4L2-KO downregulated alanyl-tRNA synthetase 1 (AARS1) (Fig. 4a), a lactate sensor mediating lactylation[32], and reduced lactate levels (Fig. 4b). Also, immunoprecipitation demonstrated significantly lower AIM2 lactylation in knockout cells (Fig. 6n), which may be related to its induction effect on PANoptosis. In summary, NDUFA4L2-KO combined with cisplatin can reduce lactate levels by inhibiting tumor cells glycolysis, thereby suppressing AIM2 lactylation and inducing tumor cells to undergo PANoptosis (Fig. 6o).

3. Discussion

Chemotherapy is an effective treatment strategy for HNSCC, but resistance to it can lead to treatment failure. The molecular mechanism of HNSCC cisplatin resistance is complex, involving cancer stem cells, autophagy, epithelial-mesenchymal transition, drug metabolism, DNA repair processes, epigenetic regulation, evasion of apoptosis, metabolic reprogramming, and influences on the tumor microenvironment[33]. Therefore, exploring ways to overcome HNSCC chemotherapy resistance is of critical importance. Our findings indicate that high expression of NDUFA4L2 in HNSCC is associated with poor prognosis and chemotherapy resistance. NDUFA4L2-KO can decrease AIM2 lactylation levels by inhibiting tumor glycolysis, thereby promoting tumor cell PANoptosis, enhancing the immune microenvironment, and ultimately augmenting the efficacy of cisplatin treatment.

NDUFA4L2 was first reported in 2011 as a target gene of HIF-1α. Since then, an increasing number of studies have found that NDUFA4L2 plays a critical role in various cancers[34,35]. Notably, NDUFA4L2 overexpression has been consistently associated with chemoresistance across multiple tumor types[36,37]. However, the role of NDUFA4L2 in HNSCC remains unclear. This study, through bioinformatics analysis and detection of clinical HNSCC samples, found that NDUFA4L2 is high expression in HNSCC, especially in chemotherapy-resistant patients. Moreover, high expression of NDUFA4L2 is associated with pathways such as hypoxia and apoptosis in HNSCC cells, and can lead to a poorer survival rate. *In vivo* and *in vitro* experiments demonstrated that NDUFA4L2-KO can induce PANoptosis, significantly enhancing the therapeutic efficacy of cisplatin.

In cancer, dysregulated cell death signaling allows cancer cells to evade PCD, leading to uncontrolled proliferation, treatment resistance, and cancer recurrence[38]. PANoptosis is a newly discovered form of regulated cell death. Inducing PANoptosis may have broad applications in eliminating various types of cancer cells while activating durable immune protection[39,40]. Therefore, exploring the PANoptosis pathway plays an important role in combating drug resistance. AIM2 is an upstream receptor of pyroptosis, cell death, and necroptosis, and participates in driving PANoptosis[41]. Wang et al. found that DNASE1L3 can activate the AIM2 pathway to induce PANoptosis, thereby enhancing the therapeutic efficacy of sorafenib and PD-1 mAb combination therapy, and remodeling the tumor immune microenvironment (TME)[42]. In our experiment, we examined markers associated with PANoptosis in HNSCC cells. We discovered that NDUFA4L2-KO cells exhibited robust PANoptosis, particularly when combined with cisplatin therapy, simultaneously activating apoptosis, pyroptosis, and necroptosis. This led us to conclude that NDUFA4L2-KO can enhance anti-tumor and anti-drug resistance effects by promoting the PANoptosis pathway. Subsequently, we found that NDUFA4L2 knockout significantly elevated AIM2 protein levels in both cisplatin-treated HNSCC cells and mouse tumor models. This was accompanied by strengthened AIM2-ASC interactions and enhanced associations with RIPK1 and CASPASE-8, confirming AIM2-PANoptosome activation. Conversely, AIM2 knockdown attenuated the cytotoxic effects of NDUFA4L2 knockout plus cisplatin treatment. The combination therapy additionally improved the tumor immune microenvironment in mice. This indicates that NDUFA4L2-KO promotes cisplatin efficacy by inducing PANoptosis of HNSCC in an AIM2-dependent manner.

Elevated aerobic glycolysis has been shown to promote tumor cell proliferation and chemotherapy resistance[43,44]. Through RNA sequencing, we observed that knockout of NDUFA4L2 could suppress glycolysis-related genes in HNSCC cells, thereby inhibiting the development and drug resistance of HNSCC. However, although many studies have demonstrated that inhibition of glycolysis can promote cancer cell apoptosis[45,46], we still know little about the association between glycolysis and PANoptosis. Thus, we conducted a preliminary investigation that included both *in vivo* and *in vitro* experiments. The results revealed that the use of a glycolysis inhibitor could also activate PANoptosis in HNSCC, thereby enhancing cisplatin efficacy. This indicates a definite link between glycolysis and PANoptosis. Moreover, the promotion of PANoptosis by knockout of NDUFA4L2 could be achieved through the inhibition of glycolysis. Future studies can further explore the specific molecular mechanism by which knockout of NDUFA4L2 inhibits glycolysis.

Lactate is a byproduct of glycolysis, and it can also promote chemotherapy resistance[47,48], as well as lead to an immunosuppressive microenvironment within neoplasms[49,50]. Moreover, the accumulation of lactate can induce a recently discovered post-translational modification—lactylation. In addition to remodeling chromatin and epigenetic regulation of gene expression through histone lactylation[51], lactylation also modifies effector proteins, altering their functions and interactions[52]. Our study demonstrates that NDUFA4L2 knockout suppresses glycolysis, reducing intracellular lactate levels. RNA sequencing revealed concomitant downregulation of alanyl-tRNA synthetase 1 (AARS1), a lactate-sensing enzyme mediating lactylation, suggesting lactylation's potential role in PANoptosis regulation. Notably, cisplatin treatment combined with NDUFA4L2 knockout specifically upregulated AIM2 (but not ZBP1 or NLRP3), which was essential for PANoptosis induction. Subsequent analysis showed NDUFA4L2 knockout significantly decreased AIM2 lactylation. We propose that AIM2 lactylation may impair PANoptosome assembly through unidentified mechanisms, positioning AIM2 delactylation as a promising therapeutic strategy to potentiate tumor cell PANoptosis. Currently, no studies have investigated the structural, spatial, or biochemical basis of AIM2-specific lactylation changes - a critical knowledge gap our team will address in future research to elucidate how AIM2 delactylation mechanistically regulates PANoptosis.

In summary, this study confirms that the NDUFA4L2 gene can promote the progression of head and neck squamous cell carcinoma (HNSCC) and enhance cisplatin chemotherapy resistance. By inhibiting glycolysis, knockout of the NDUFA4L2 gene can mediate AIM2 delactylation and induce a widespread apoptosis process in tumors, as well as regulate the tumor microenvironment. This indicates that NDUFA4L2 is a highly promising target for suppressing the development of head and neck squamous cell carcinoma and chemotherapy drug resistance, and further in-depth research on it may provide new strategies to improve chemotherapy efficacy.

4. Methods

4.1. Ethical statements

The study was approved by Nanjing Medical University Ethics Committee (PJ2023-147-001) with participants' written consent, following Helsinki Declaration guidelines. All Animal

Experiments were conducted per IACUC-approved protocols (IACUC-2409093) in SPF facilities of Nanjing Medical University.

4.2. Bioinformatics data collection and analysis

To identify conserved transcriptional programs in tumor cells, we employed a cross-sample NMF analysis strategy. Public HNSCC scRNA-seq datasets (GSE181919, GSE234933, GSE211630) were analyzed. Initial processing involved quality control, normalization, dimensionality reduction, and preliminary cell typing using Seurat. Cells were filtered (1,000-4,000 UMIs; 300-6,000 expressed genes; <15% mitochondrial content), followed by Harmony-based batch correction. Following PCA-based dimensionality reduction, tumor cells were identified using Seurat's FindClusters function and segregated by sample into a list of datasets. For each sample, multiNMF was applied to the SCT-normalized expression matrix (assay="SCT", slot="data") using 5,000 highly variable genes and testing the number of modules k ranging from 4 to 10. Conserved meta-programs were extracted via getMetaPrograms, with nMP=8 selected for optimal biological specificity after parameter comparison. Cell types were annotated using literature-curated marker genes, and tumor cell subpopulations were visualized through UMAP. The stability of transcriptional modules was validated in independent datasets (GSE164690 and GSE195832), and functional annotation was conducted through enrichment analysis. Survival correlations were assessed using Kaplan-Meier analysis on bulk transcriptomic data (including TCGA cohorts) with clinical follow-up.

4.3. Tumor specimens and Animal models

The study utilized matched human tissue specimens from Nanjing Medical University's Stomatological Hospital, comprising: (1) Ten normal/HNSCC pairs across clinical stages; (2) Six chemotherapy-sensitive/resistant pairs (fresh and FFPE). Information regarding the the HNSCC patients included in this study are listed in Table 1.

Female C57BL/6 mice (6 weeks old) from Nanjing Medical University, China were randomly allocated to control or experimental groups. Tongue orthotopic xenografts were established by injecting 5×10^5 NDUFA4L2-knockout or wild-type MOC1 cells. From day 7 post-inoculation, tumor volume and body weight were monitored biweekly. Mice received intraperitoneal injections of 5 mg/kg cisplatin (ST1164, Beyotime, Shanghai, China) or 100 mg/kg 2-DG (MC8002, Meilunbio, Dalian, China). Cohort 1 underwent four treatment cycles before sacrifice on day 17 for tumor collection, while cohort 2 continued therapy until day 30 for survival analysis.

Time inducible tissue-specific *Tgfbr1/Pten* 2cKO mice (*K14-Cre$^{ERtam+/-}$; Tgfbr1$^{flox/flox}$; Pten$^{flox/flox}$*, 6-8 weeks old, FVBN/CD1/129/C57 mixed background) were provided by Prof. Zhi-Jun Sun(Wuhan University, China). After 5-day tamoxifen induction (2 mg/day in corn oil), head and neck tumor progression was tracked triweekly from day 16. Treatment protocols mirrored the C57BL/6 cohort. All mice were sacrificed on day 28 for tumor harvest, with early termination criteria being >150 mm^3 tumor volume or >20% body weight loss.

4.4. Immunohistochemistry (IHC) assay

Paraffin embedding, sectioning, Deparaffinization, and Rehydration. IHC employed microwave antigen retrieval (citrate solution or EDTA solution) followed by UltraSensitive™ SP staining kit (KIT-9706/9701, Maixin Biotech, Fuzhou, China) per manufacturer's protocol. Visualization used DAB chromogen (DAB-2031, Maixin Biotech) with hematoxylin counterstain.

4.5. Multiplex immunohistochemistry (mIHC) assay

Multiplex fluorescence immunohistochemistry kit (10217100050, PANOVUE, Beijing, China) with tyramide signal amplification across six fluorescence channels (PPD480, PPD520, PPD570, PPD620, PPD650, PPD780) was used. Nuclei were counterstained with DAPI (P0131, Beyotime) in antifade mounting medium.

4.6. Cell lines

The human OSCC lines WSU-HN30 (HN30), HN6, and normal oral keratinocytes HOK were sourced from Shanghai Ninth People's Hospital. Human tongue squamous cell carcinoma cell line CAL27 (TCH-C148) and human pharyngeal squamous cell carcinoma cell line FaDu (TCH-C174) were obtained from Haixing Bio, Fujian, China. The murine OSCC line MOC1 (EWL001-FP, Kerafast, MA, USA) was obtained commercially. HN6, HN30, HOK, CAL27 cells were cultured in Dulbecco's modified Eagle's medium (DMEM; GIBCO, Grand Island, NY, USA) with 10% fetal bovine serum (GIBCO), 1% Penicillin-Streptomycin Solution (Haixing Bio). FaDu cell were cultured in Minimum Essential Medium (MEM) (GIBCO) with 10% fetal bovine serum (GIBCO), 1% Penicillin-Streptomycin Solution (Haixing Bio). MOC1 cell were cultured in Iscove's Modified Dulbecco's Medium (IMDM; GIBCO)/Ham's Nutrient Mixture F12 (GIBCO) at a 2:1 mixture with 5% fetal bovine serum (GIBCO), 1% Penicillin-Streptomycin Solution (Haixing Bio), 5 ng/mL epidermal growth factor (EGF; EMD Millipore Corporation, Temecula, CA, USA), 400 ng/mL hydrocortisone (Sigma Aldrich, St Louis, MO, USA), and 5 mg/mL insulin (Sigma Aldrich). All cells were cultured in a 37°C, 5% CO_2 incubator and tested negative for mycoplasma contamination detection.

4.7. Cell transfection

NDUFA4L2-knockout lentivirus was generated by cloning validated sgRNAs into pLV1cmv-Cas9-Puro-U6 (Corues Nanjing, China). After being packagd in 293T cells, viral particles (MOI=10) with 8 μg/mL Polybrene were used to transduce CAL27, FaDu, organoids, and MOC1 in antibiotic-free medium. Selection with 1 μg/mL puromycin (HY-B1743, MedChemExpress, UJ, USA) began 24h post-transduction. Knockout efficiency was quantified at 48-72h by RT-qPCR and Western blot analysis. sgRNA sequences were as follows:
sgNDUFA4L2-1(human): GTAGAAGCGGGCCCCAAGAC,
sgNdufa4l2-1(mouse): AAGATGGCAGGAACTAGTCT,
sgNdufa4l2-2(mouse): TGGCTTCATCTGCTTGGGCA,
sgNdufa4l2-3(mouse): ACCAGACATCAGGACTGCGC.

The siRNA vectors were synthesized from Corues Nanjing, China. Cells were plated 24 hours before transfection and transfected with 100 nM siRNA. Transfection was conducted in a 2 mL

serum-free medium system using Lipofectamine 3000 (Thermo Fisher, USA) per manufacturer's protocol, with an initial 8-hour incubation. Following medium replacement, cells were cultured for an additional 48 hours. The si-AIM2 targeting sequence was: GGAAGGAAGACAAGAGAUATT(mouse); GAACAAUUGUGAAUGGUUUTT(human).

4.8. CCK-8 Assay Protocol

Cells were plated in a 96-well plate and treated with cisplatin or 2-DG at gradient concentrations for 24 h post-attachment. The IC_{50} was determined by measuring optical density (OD). Cells were then cultured with IC_{50}-dose cisplatin for 3 days, with daily OD measurements to generate growth curves. Prior to measurement, the medium was replaced with 100 μL of fresh medium containing 10% CCK-8 reagent (MA0218, Meilunbio, Dalian, China). After 1 h incubation, OD450 was quantified using a microplate reader.

4.9. Live/Dead Cell Assay

Cell viability and cytotoxicity were assessed using the Calcein/PI Cell Viability/Cytotoxicity Assay Kit (C2015, Beyotime, Shanghai, China). Following drug treatment in 24-well plates, cells were incubated with the assay reagents and examined under a fluorescence microscope. Under fluorescence observation, live cells appeared green, while dead cells were stained red.

4.10. Organoids construction

After multiple washes with PBS containing Dual Antibiotics, the samples were minced and incubated in Tumor Tissue Digestion Solution (K60103, Biogenous, Jiangsu, China). The resulting suspension was filtered and centrifuged, after which the supernatant was discarded. The pellet was subsequently washed with Cancer Organoid Basal Medium (B213152, Biogenous) and embedded in chilled Matrigel (34234, Corning, NY, USA), before being seeded into 24-well plates. Organoid Complete Medium (K2152-OSC, Biogenous) was added after the matrigel had polymerized.

4.11. Flow cytometry

On day 17 following the injection of MOC1 cells, mice were euthanized, and tumor tissue was collected and dissociated into a single-cell suspension using the Miltenyi autoMACS Pro Dissociator. The resulting cell suspension was stained with Fluorescently Labeled Antibody and subsequently analyzed by flow cytometry. Data visualization and analysis were conducted using FlowJo Software (version 10.9.0). All staining procedures were performed strictly in accordance with the protocols provided by the respective manufacturers. The antibody panel used for staining is listed below.

Zombie Aqua™ dye 405（1:1000；Biolegend，CA，USA）
Anti-CD45-APC-Cy7（1:500；eBioscience，CA，USA）
Anti-CD3-FITC（1:500；Biolegend，CA，USA）
Anti-CD8-PerCP-Cy5.5（1:500；Biolegend，CA，USA）
Anti-CD11b-FITC（1:500；Biolegend，CA，USA）
Anti-F4/80-PerCP-Cy5.5（1:500；Biolegend，CA，USA）

Anti-CD206-APC（1:200；Biolegend，CA，USA）

4.12. RNA extraction and RNA-seq

Total RNA was isolated from cultured cells using RNA isolater Total RNA Extraction Reagent (R401-01, Vazyme, Jiangsu, China). cDNA synthesis was performed with HiScript II All-in-one RT SuperMix Perfect for qPCR Kit (R333, Vazyme, Jiangsu, China). Quantitative PCR analysis employed ChamQ Universal SYBR qPCR Master Mix Kit (Vazyme, Nanjing, China), with β-actin as the endogenous control. Target gene expression levels were calculated via the $2^{-\Delta\Delta CT}$ method. Primer sequences are provided below.

NDUFA4L2:
Forward: CGCTTTACTTGCTGCGACTC.
Reverse: GTGGAAACTGCAAGGAACTTGT;
AIM2:
Forward: TCTCCTGAGTCCTCTGCTAGT.
Reverse: CCGATTTGTATTGCTTATCAACTCC;
β-Actin:
Forward: CTCGCCTTTGCCGATCC.
Reverse: ATCCTTCTGACCCATGCCC.

RNA was extracted from FaDu cells transfected with sg-RNA and negative control, followed by RNA-seq. The RNA-seq and subsequent data analysis were carried out by Metware, Wuhan, China. All samples were processed in triplicate.

4.13. Western Blotting Analysis

Cell lysates were prepared with RIPA lysis buffer (P0013B, Beyotime). Protein concentration was quantified using the Enhanced BCA Protein Assay Kit (P0010S, Beyotime) per the manufacturer's protocol. Proteins were resolved via SDS-PAGE using the Omni-Easy™ One-step Color PAGE Gel Rapid Preparation Kit (PG-212, Epizyme, Shanghai, China) and Tris-Glycine SDS-PAGE SWE high-resolution buffer (G2081-15, Servicebio, Wuhan, China), then electroblotted onto a 0.45 μm PVDF membrane (IPVH00010, Millipore, Boston, MA, USA). The membrane was blocked for 15 min at RT with QuickBlock™ Blocking Buffer (P0252, Beyotime), followed by overnight incubation with primary antibody at 4°C. After three washes, HRP-conjugated secondary antibody (7074P2/7076P2, Cell Signaling Technology, Danvers, MA, USA) was applied, and signals were detected using ECL substrate (BL520, Biosharp, Anhui, China).

4.14. Immunoprecipitation (IP) assay

Cells were lysed on ice for 30 minutes using Cell lysis buffer for Western and IP (P0013, Beyotime) supplemented with PMSF Solution (ST507, Beyotime). After protein concentrations were determined using the Enhanced BCA Protein Assay Kit (P0010S, Beyotime), the resulting lysates were incubated in the presence of magnetic protein A/G beads (HY-K0202, MedChemExpress, UJ, USA) and the appropriate primary antibody. Normal immunoglobulin (IgG) served as the negative IP control. Then the beads were washed at least five times and boiled to

elute the bound proteins for subsequent Western blot analysis.

Details of the primary antibody used in this study are listed in Table 2.

4.15. Statistical analysis

GraphPad Prism 10.0 (GraphPad Software, Inc., La Jolla, CA, USA) was applied in statistical analysis. Unpaired or paired *t* tests were adopted for data between two groups. Two-way ANOVA was used for data between multiple groups. Data are represented as the mean ± standard deviation (*S.D.*). Significance was determined as $P < 0.05$.

Data Availability

All data relevant to the study are included in the article or uploaded as supplementary information. Additional supporting data are available from the corresponding authors upon reasonable request, and the raw sequence data reported in this paper have been deposited in the Genome Sequence Archive (Genomics, Proteomics & Bioinformatics 2025) in National Genomics Data Center (Nucleic Acids Res 2025), China National Center for Bioinformation / Beijing Institute of Genomics, Chinese Academy of Sciences[53,54] (GSA-Human: HRA013828) that are publicly accessible at https://ngdc.cncb.ac.cn/gsa-human.

Code Availability

All analyses were performed using conventional analysis code, which is available at https://github.com/carmonalab/GeneNMF,[55] and no new codes were generated.

Acknowledgments

We acknowledge Yongchu Pan, Mifang Yang, Dongling Yan, and Linlin Jiang for the use of experimental instruments (Jiangsu Key Laboratory of Oral Diseases, Nanjing Medical University). The authors thank Prof. Zhi-Jun Sun for the kind gift of the time inducible tissue-specific Tgfbr1/Pten 2cKO HNSCC mice. This research was funded by the Natural Science Foundation of the Jiangsu Higher Education Institutions of China (Grant No. 23KJA320003).

Author contributions

J.J.C.: Data curation, conceptualization, methodology, formal analysis, investigation, writing-original draft. **Y.Y.:** Data curation, methodology, formal analysis, investigation, writing-original draft. **J.H.Z.:** Data curation, formal analysis, methodology, investigation. **Y.J.G.:** Data curation, formal analysis, methodology. **M.R.Z.:** Data curation, formal analysis, investigation. **R.Z.:** Data curation, methodology. **Y.H.L.:** Investigation. **J.Y.W.:** Investigation. **X.S.:** Conceptualization, supervision, funding acquisition, project administration, resources, writing-review, and editing.

Competing Interests

The authors declare no competing financial or non-financial interests.

References

1. Johnson, D. E. et al. Head and neck squamous cell carcinoma. *Nat. Rev. Dis. Primers*. **6**, 92 10.1038/s41572-020-00224-3(2020).
2. Barsouk, A., Aluru, J. S., Rawla, P., Saginala, K. & Barsouk, A. Epidemiology, Risk Factors, and Prevention of Head and Neck Squamous Cell Carcinoma. *Med Sci (Basel)*. **11**, 10.3390/medsci11020042(2023).
3. Galluzzi, L. et al. Molecular mechanisms of cisplatin resistance. *Oncogene*. **31**, 1869-1883 10.1038/onc.2011.384(2012).
4. Peng, F. et al. Regulated cell death (RCD) in cancer: key pathways and targeted therapies. *Signal Transduct. Target. Ther.* **7**, 286 10.1038/s41392-022-01110-y(2022).
5. Wu, D., Wang, S., Yu, G. & Chen, X. Cell Death Mediated by the Pyroptosis Pathway with the Aid of Nanotechnology: Prospects for Cancer Therapy. *Angew Chem Int Ed Engl*. **60**, 8018-8034 10.1002/anie.202010281(2021).
6. Bedoui, S., Herold, M. J. & Strasser, A. Emerging connectivity of programmed cell death pathways and its physiological implications. *Nat. Rev. Mol. Cell Biol.* **21**, 678-695 10.1038/s41580-020-0270-8(2020).
7. Malireddi, R. K. S., Kesavardhana, S. & Kanneganti, T. ZBP1 and TAK1: Master Regulators of NLRP3 Inflammasome/Pyroptosis, Apoptosis, and Necroptosis (PAN-optosis). *Front. Cell. Infect. Microbiol.* **9**, 406 10.3389/fcimb.2019.00406(2019).
8. Lee, S. et al. AIM2 forms a complex with pyrin and ZBP1 to drive PANoptosis and host defence. *Nature*. **597**, 415-419 10.1038/s41586-021-03875-8(2021).
9. Cridland, J. A. et al. The mammalian PYHIN gene family: phylogeny, evolution and expression. *BMC Evol. Biol.* **12**, 140 10.1186/1471-2148-12-140(2012).
10. Zhang, M., Zhang, L., Miao, T. & Hu, X. Characterization of PANoptosis-related expression pattern, prognosis and tumor microenvironment in head and neck squamous cell carcinoma. *Discov Oncol*, 10.1007/s12672-025-04328-8(2025).
11. Yang, P. et al. Identification of PANoptosis-related biomarkers and analysis of prognostic values in head and neck squamous cell carcinoma. *Sci. Rep.* **14**, 9824 10.1038/s41598-024-60441-8(2024).

12. Tello, D. et al. Induction of the mitochondrial NDUFA4L2 protein by HIF-1alpha decreases oxygen consumption by inhibiting Complex I activity. *Cell Metab.* **14**, 768-779 10.1016/j.cmet.2011.10.008(2011).
13. Lai, R. K. et al. NDUFA4L2 Fine-tunes Oxidative Stress in Hepatocellular Carcinoma. *Clin. Cancer Res.* **22**, 3105-3117 10.1158/1078-0432.CCR-15-1987(2016).
14. Ye, N. et al. Hypoxia-induced the upregulation of NDUFA4L2 promoted colon adenocarcinoma progression through ROS-mediated PI3K/AKT pathway. *Cytotechnology*. **75**, 461-472 10.1007/s10616-023-00590-2(2023).
15. Meng, L., Yang, X., Xie, X. & Wang, M. Mitochondrial NDUFA4L2 protein promotes the vitality of lung cancer cells by repressing oxidative stress. *Thorac. Cancer*. **10**, 676-685 10.1111/1759-7714.12984(2019).
16. Yuan, Y. et al. NDUFA4L2 promotes trastuzumab resistance in HER2-positive breast cancer. *Ther. Adv. Med. Oncol.* **13**, 17527428 10.1177/17588359211027836(2021).
17. Wang, D., Zhang, P., Liu, Z., Xing', Y. & Xiao, Y. NXPH4 Promotes Gemcitabine Resistance in Bladder Cancer by Enhancing Reactive Oxygen Species and Glycolysis Activation through Modulating NDUFA4L2. *Cancers*. **14**, 10.3390/cancers14153782(2022).
18. Zhou, L. et al. Transcriptional regulation of NDUFA4L2 by NFIB induces sorafenib resistance by decreasing reactive oxygen species in hepatocellular carcinoma. *Cancer Sci.* **114**, 793-805 10.1111/cas.15648(2023).
19. Chamoli, A. et al. Overview of oral cavity squamous cell carcinoma: Risk factors, mechanisms, and diagnostics. *Oral Oncol.* **121**, 105451 10.1016/j.oraloncology.2021.105451(2021).
20. Warburg, O., Wind, F. & Negelein, E. THE METABOLISM OF TUMORS IN THE BODY. *J. Gen. Physiol.* **8**, 519-530 10.1085/jgp.8.6.519(1927).
21. Vander Heiden, M. G., Cantley, L. C. & Thompson, C. B. Understanding the Warburg effect: the metabolic requirements of cell proliferation. *Science*. **324**, 1029-1033 10.1126/science.1160809(2009).
22. Li, F. et al. Acetylation accumulates PFKFB3 in cytoplasm to promote glycolysis and protects cells from cisplatin-induced apoptosis. *Nat. Commun.* **9**, 508 10.1038/s41467-018-02950-5(2018).
23. Faes, S. et al. Acidic tumor microenvironment abrogates the efficacy of mTORC1 inhibitors. *Mol. Cancer*. **15**, 78 10.1186/s12943-016-0562-y(2016).
24. Lin, Y. et al. Knockdown of PKM2 enhances radiosensitivity of cervical cancer cells. *Cancer Cell Int.* **19**, 129 10.1186/s12935-019-0845-7(2019).
25. Zong, S., Dai, W., Fang, W., Guo, X. & Wang, K. SIK2 Promotes Cisplatin Resistance Induced by Aerobic Glycolysis in Breast Cancer Cells through PI3K/AKT/mTOR Signaling Pathway. *Biosci. Rep.*, 10.1042/BSR20201302(2020).
26. Tan, Y. et al. Pyroptosis: a new paradigm of cell death for fighting against cancer. *J. Exp. Clin. Cancer Res.* **40**, 153 10.1186/s13046-021-01959-x(2021).
27. Slee, E. A. et al. Benzyloxycarbonyl-Val-Ala-Asp (OMe) fluoromethylketone (Z-VAD.FMK) inhibits apoptosis by blocking the processing of CPP32. *Biochem. J.* **315 (Pt 1)**, 21-24 10.1042/bj3150021(1996).
28. Xu, W. et al. Gasdermin E-derived caspase-3 inhibitors effectively protect mice from acute hepatic failure. *Acta Pharmacol. Sin.* **42**, 68-76 10.1038/s41401-020-0434-2(2021).
29. Cao, L. & Mu, W. Necrostatin-1 and necroptosis inhibition: Pathophysiology and therapeutic implications. *Pharmacol. Res.* **163**, 105297 10.1016/j.phrs.2020.105297(2021).
30. Wang, Y. et al. Chemotherapy drugs induce pyroptosis through caspase-3 cleavage of a gasdermin. *Nature*. **547**, 99-103 10.1038/nature22393(2017).
31. Yu, X. & He, S. GSDME as an executioner of chemotherapy-induced cell death. *Sci. China Life Sci.* **60**, 1291-1294 10.1007/s11427-017-9142-2(2017).

32. Zong, Z., Ren, J., Yang, B., Zhang, L. & Zhou, F. Emerging roles of lysine lactyltransferases and lactylation. *Nat. Cell Biol.* **27**, 563-574 10.1038/s41556-025-01635-8(2025).
33. Hu, H. et al. New advances into cisplatin resistance in head and neck squamous carcinoma: Mechanisms and therapeutic aspects. *Biomed. Pharmacother.* **163**, 114778 10.1016/j.biopha.2023.114778(2023).
34. Mei, Q. et al. Elevated of NDUFA4L2 expression in colon adenocarcinoma is correlated with an unfavorable prognosis and increased immune cell infiltration. *Heliyon*. **10**, e25462 10.1016/j.heliyon.2024.e25462(2024).
35. Lv, Y. et al. Overexpression of NDUFA4L2 is associated with poor prognosis in patients with colorectal cancer. *ANZ J. Surg.* **87**, E251-E255 10.1111/ans.13617(2017).
36. He, H. et al. Nucleotide metabolism-associated drug resistance gene NDUFA4L2 promotes colon cancer progression and 5-FU resistance. *Sci. Rep.* **15**, 570 10.1038/s41598-024-84353-9(2025).
37. Li, L. et al. The identification of induction chemo-sensitivity genes of laryngeal squamous cell carcinoma and their clinical utilization. *Eur. Arch. Otorhinolaryngol.* **275**, 2773-2781 10.1007/s00405-018-5134-x(2018).
38. Mohammad, R. M. et al. Broad targeting of resistance to apoptosis in cancer. *Semin. Cancer. Biol.* **35 Suppl**, S78-S103 10.1016/j.semcancer.2015.03.001(2015).
39. Zhu, P. et al. Advances in mechanism and regulation of PANoptosis: Prospects in disease treatment. *Front. Immunol.* **14**, 1120034 10.3389/fimmu.2023.1120034(2023).
40. Malireddi, R. K. S., Tweedell, R. E. & Kanneganti, T. PANoptosis components, regulation, and implications. *Aging (Albany NY)*. **12**, 11163-11164 10.18632/aging.103528(2020).
41. Sagulenko, V. et al. AIM2 and NLRP3 inflammasomes activate both apoptotic and pyroptotic death pathways via ASC. *Cell Death Differ.* **20**, 1149-1160 10.1038/cdd.2013.37(2013).
42. Wang, J. et al. DNASE1L3-mediated PANoptosis enhances the efficacy of combination therapy for advanced hepatocellular carcinoma. *Theranostics*. **14**, 6798-6817 10.7150/thno.102995(2024).
43. Gao, W. et al. Targeting SKA3 suppresses the proliferation and chemoresistance of laryngeal squamous cell carcinoma via impairing PLK1-AKT axis-mediated glycolysis. *Cell Death Dis.* **11**, 919 10.1038/s41419-020-03104-6(2020).
44. Wang, L. et al. Wnt1-inducible signaling protein 1 regulates laryngeal squamous cell carcinoma glycolysis and chemoresistance via the YAP1/TEAD1/GLUT1 pathway. *J. Cell. Physiol.* **234**, 15941-15950 10.1002/jcp.28253(2019).
45. Rastogi, S., Banerjee, S., Chellappan, S. & Simon, G. R. Glut-1 antibodies induce growth arrest and apoptosis in human cancer cell lines. *Cancer Lett.* **257**, 244-251 10.1016/j.canlet.2007.07.021(2007).
46. Munoz-Pinedo, C., Ruiz-Ruiz, C., Ruiz De Almodovar, C., Palacios, C. & Lopez-Rivas, A. Inhibition of glucose metabolism sensitizes tumor cells to death receptor-triggered apoptosis through enhancement of death-inducing signaling complex formation and apical procaspase-8 processing. *J. Biol. Chem.* **278**, 12759-12768 10.1074/jbc.M212392200(2003).
47. Sun, F. et al. Impact of glycolysis enzymes and metabolites in regulating DNA damage repair in tumorigenesis and therapy. *Cell Commun. Signal.* **23**, 44 10.1186/s12964-025-02047-9(2025).
48. Chen, H. et al. NBS1 lactylation is required for efficient DNA repair and chemotherapy resistance. *Nature*. **631**, 663-669 10.1038/s41586-024-07620-9(2024).
49. Cong, J. et al. Dysfunction of Natural Killer Cells by FBP1-Induced Inhibition of Glycolysis during Lung Cancer Progression. *Cell Metab.* **28**, 243-255 10.1016/j.cmet.2018.06.021(2018).
50. Noe, J. T. et al. Lactate supports a metabolic-epigenetic link in macrophage polarization. *Sci. Adv.* **7**, i8602 10.1126/sciadv.abi8602(2021).
51. Zhang, D. et al. Metabolic regulation of gene expression by histone lactylation. *Nature*. **574**, 575-580 10.1038/s41586-019-1678-1(2019).

52. Liu, S. et al. Crosstalk between lactylation and RNA modifications in tumorigenesis: mechanisms and therapeutic implications. *Biomark. Res.* **13**, 110 10.1186/s40364-025-00824-9(2025).

53. Sisi Zhang et al. The GSA Family in 2025: A Broadened Sharing Platform for Multi-omics and Multimodal Data. *Genom. Proteomics Bioinformatics*. **23**, 10.1093/gpbjnl/qzaf072(2025).

54. Database Resources of the National Genomics Data Center, China National Center for Bioinformation in 2025. *Nucleic. Acids. Res.* **53**, D30-D44 10.1093/nar/gkae978(2025).

55. Barkley, D. et al. Cancer cell states recur across tumor types and form specific interactions with the tumor microenvironment. *Nat. Genet.* **54**, 1192-1201 10.1038/s41588-022-01141-9(2022).

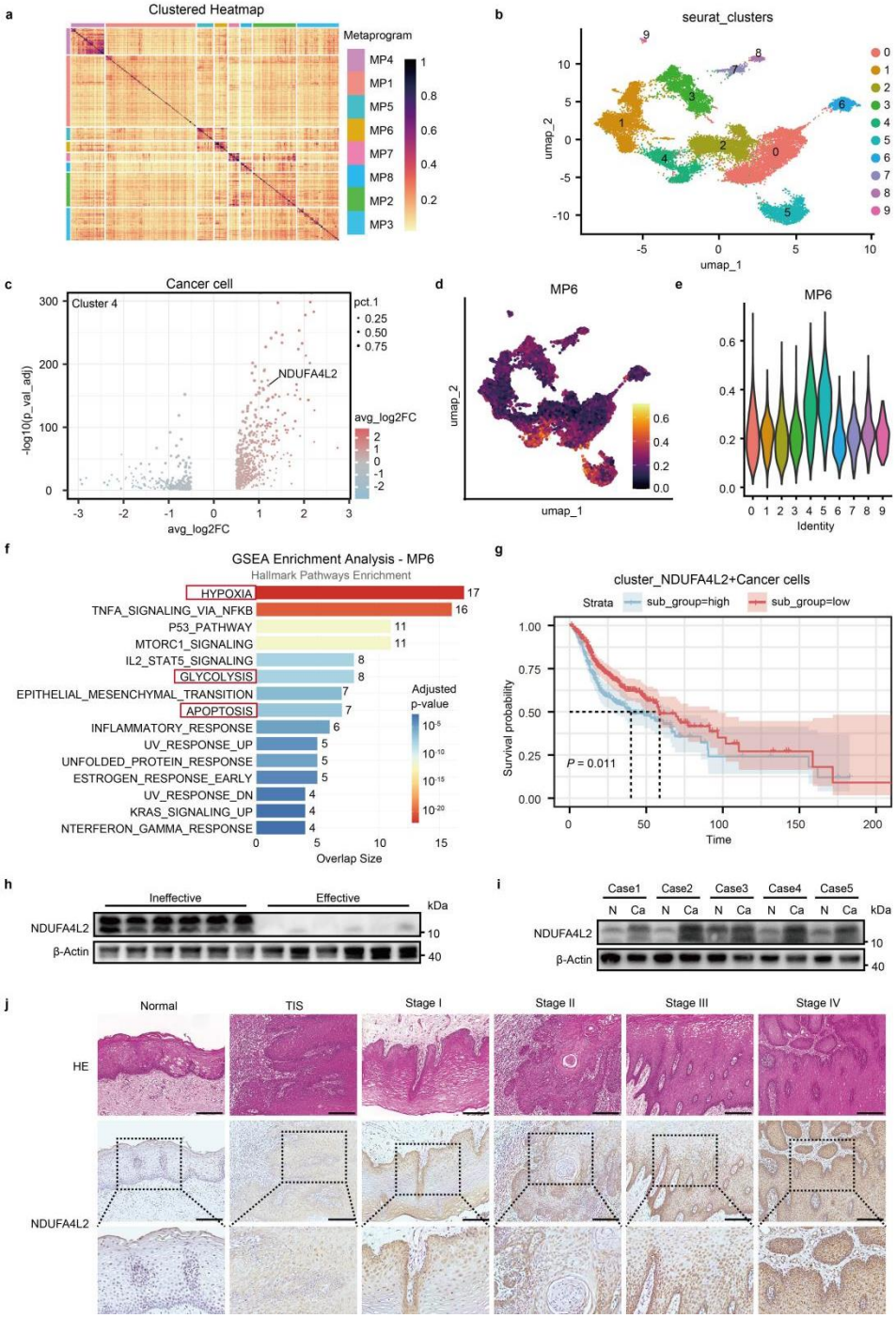

Fig. 1. Transcriptional modules and NDUFA4L2 characterization in HNSCC

(a) Hierarchically clustered correlation heatmap of transcriptional modules. **(b)** UMAP algorithm classifies HNSCC cells into ten clusters, indicated by different colors. **(c)** Volcano plot of differentially expressed genes in cluster 4. **(d)** FeaturePlot of module MP6 expression. **(e)** Violin plot showing MP6 expression across clusters. **(f)** GSEA enrichment analysis (top 15 pathways) for MP6. **(g)** Kaplan-Meier survival analysis by NDUFA4L2 expression (high vs low). **(h, i)** Western blot analysis of NDUFA4L2 in six chemotherapy-resistant vs six sensitive HNSCC tissues **(h),** five normal vs five HNSCC tissues **(i)**. **(j)** Representative IHC (NDUFA4L2) and

H&E staining in normal and staged HNSCC tissues (scale bar: 100 μm).

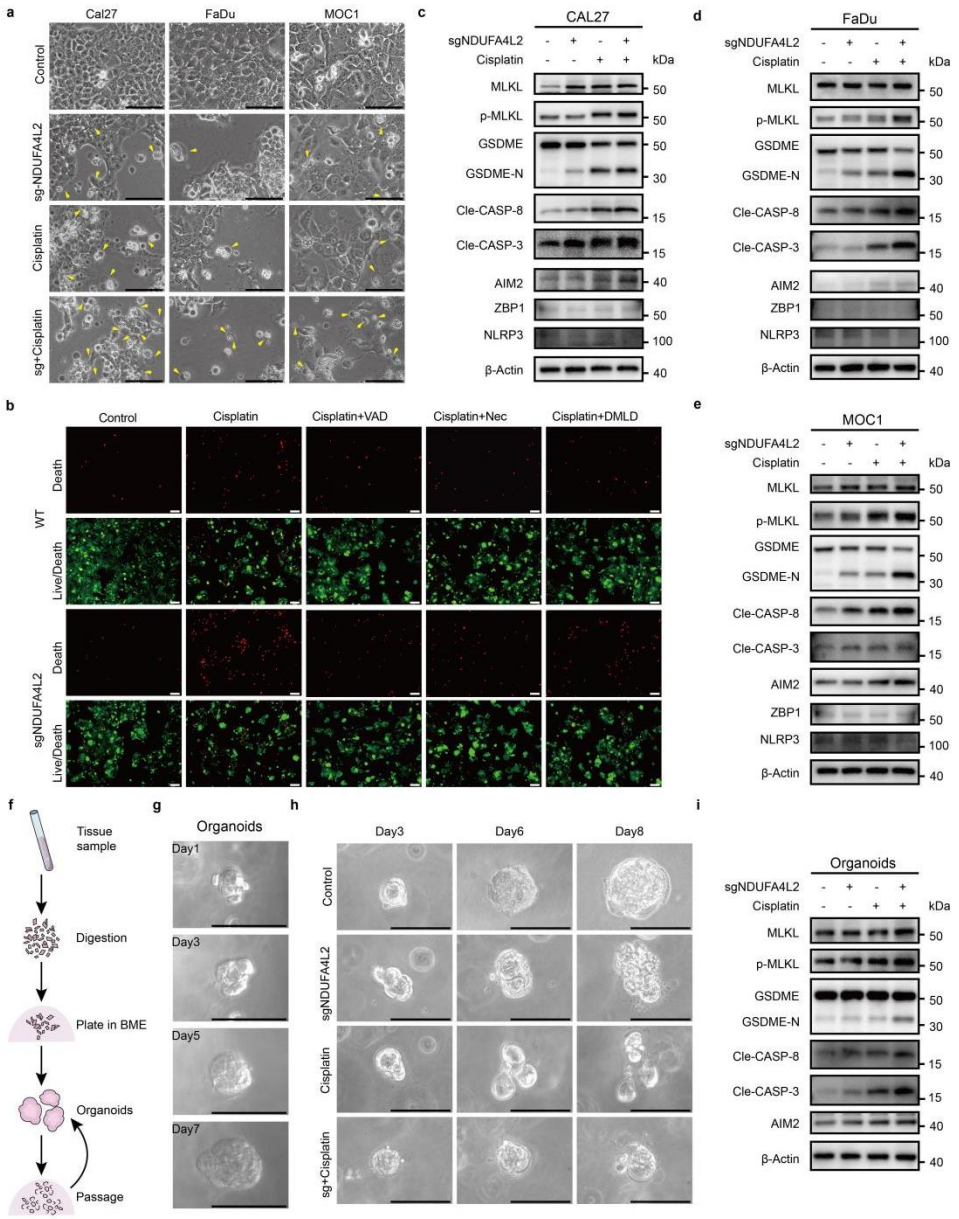

Fig. 2. NDUFA4L2 knockout enhances cisplatin-induced PANoptosis

(a) Microscopic images of control and NDUFA4L2-KO CAL27, FaDu, and MOC1 cells treated with 15 μM cisplatin (24 h). Yellow arrows indicate pyroptotic cells (scale bar: 100 μm, *n* = 3, biological replicates). **(b)** Live/dead assay (red = dead, green = live) in control and NDUFA4L2-KO CAL27 cells treated for 24 h with: cisplatin alone (15 μM), or combined with Z-VAD-FMK (25 μM), necrostatin-1 (20 μM), or Ac-DMLD-cmk (20 μM) (scale bar: 100 μm, *n* = 3, biological replicates). **(c-e, i)** Western blots of PANoptosis markers (Cleaved Caspase-3/8, p-MLKL, MLKL, GSDME, GSDME-N, AIM2, ZBP1, NLRP3) in cisplatin-treated (15 μM, 24 h) control and NDUFA4L2-KO cells/organoids. **(f, g)** OSCC organoid generation scheme and growth progression (days 1,3,5,7; scale bar: 100 μm). **(h)** Microscopic images of organoid after cisplatin treatment (15

μM, 72/120 h) in control vs NDUFA4L2-KO groups (scale bar: 100 μm, n = 3, biological replicates).

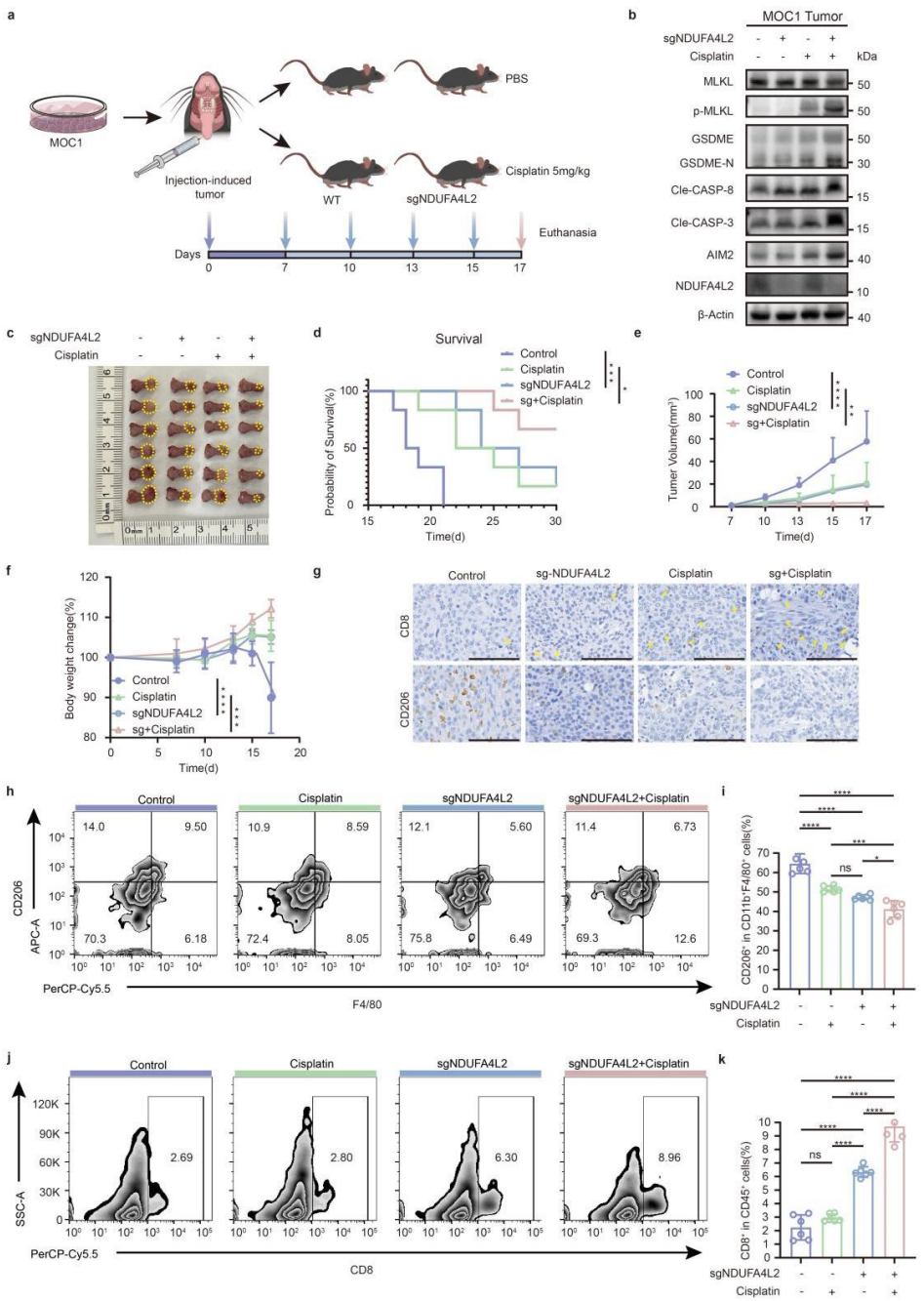

Fig. 3. NDUFA4L2 knockout enhances cisplatin efficacy *in vivo*

(a) Experimental design of MOC1 tumor inoculation followed by i.p. treatments (PBS OR cisplatin) on days 7, 10, 13 and 15. **(b)** Western blot analysis of PANoptosis markers (NDUFA4L2, Cleaved Caspase-3/8, p-MLKL, MLKL, GSDME, GSDME-N, AIM2) in tumor tissues from each group. **(c)** Macroscopic tongue tumors in C57BL/6 mice bearing control or NDUFA4L2-KO MOC1 cells after cisplatin treatment. **(d)** Survival analysis of each group. **(e, f)** Tumor growth **(e)** and body weight **(f)** curves **(g)** Representative IHC staining of $CD8^+$ T

cells and M2 macrophages in tumors (scale bar: 100 μm). **(h-k)** Flow cytometry analysis **(h)** and quantification **(i)** of M2 macrophages; Flow cytometry analysis **(j)** and quantification **(k)** of $CD8^+$ T cells. The data presented in this figure are expressed as mean ± *S.D.*; sample size, $n = 6$, biological replicates; Statistical analyses: *t*-test and two-way ANOVA. $^*P < 0.05$, $^{**}P < 0.01$; $^{***}P < 0.001$, $^{****}P < 0.0001$.

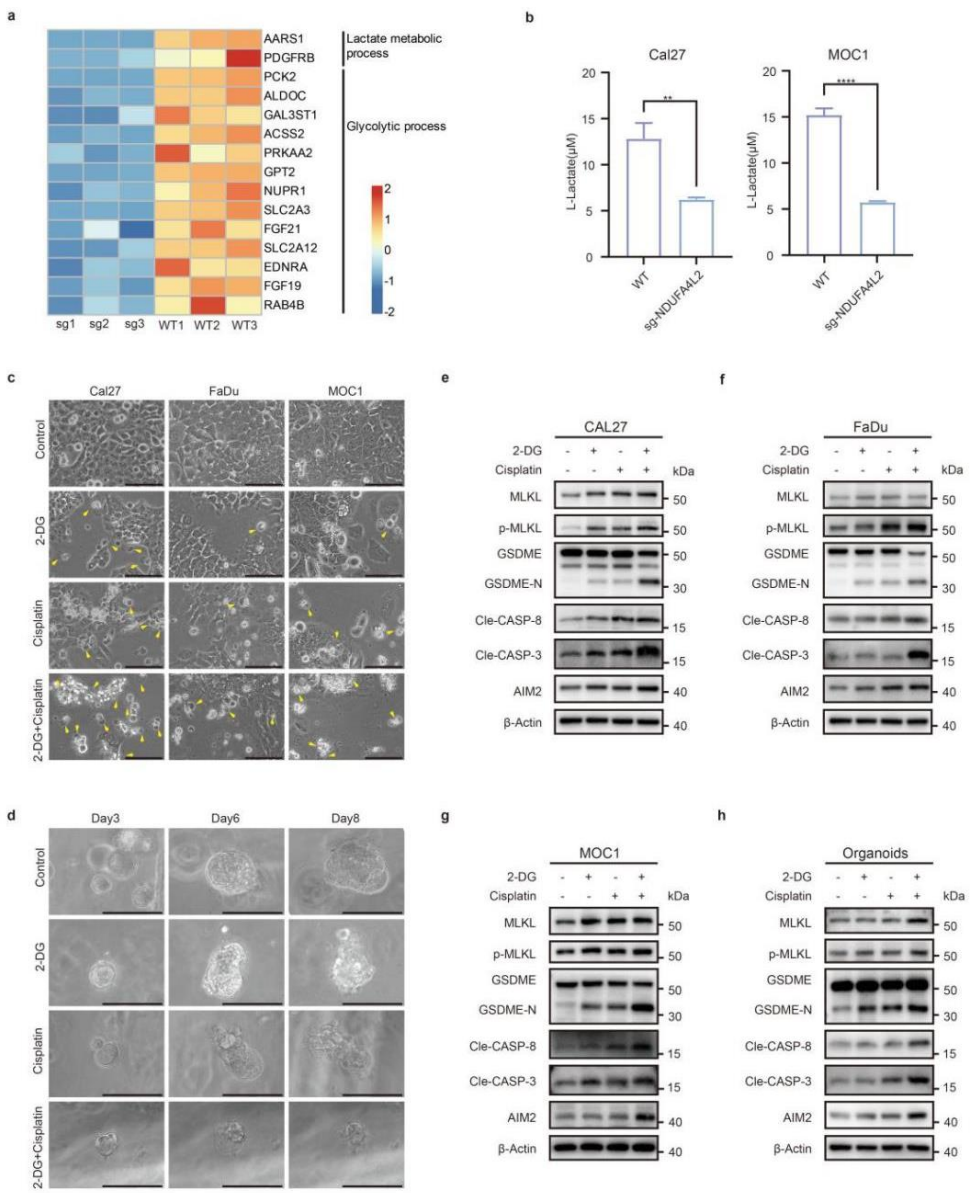

Fig. 4. NDUFA4L2-KO alters Glycolytic process and 2-DG enhances PANoptosis

(a) Heatmap of differentially expressed genes in Lactate metabolic process and Glycolytic process in control vs NDUFA4L2-KO FaDu cells (sample size, $n = 3$, biological replicates). **(b)** Intracellular lactate levels in control and NDUFA4L2-KO CAL27 and MOC1 cells (48 h culture; mean ± *S.D.*; sample size, $n = 3$, biological replicates; *t*-test; $^*P < 0.05$, $^{**}P < 0.01$; $^{***}P < 0.001$, $^{****}P < 0.0001$). **(c)** Microscopic images of CAL27, FaDu, and MOC1 cells treated for 24 h with: cisplatin (15 μM), 2-DG (3 mM), or combination (yellow arrows indicate pyroptotic cells; scale bar: 100 μm; $n = 3$, biological replicates). **(d)** Microscopic

images of organoid after treatment with cisplatin (15 μM), 2-DG (3 mM), or combination for 72/120 h (scale bar: 100 μm; *n* = 3, biological replicates). **(e-h)** Western blot analysis of PANoptosis markers (cleaved Caspase-3/8, p-MLKL, MLKL, GSDME, GSDME-N, AIM2) in cells and organoids treated for 24 h with cisplatin, 2-DG, or combination.

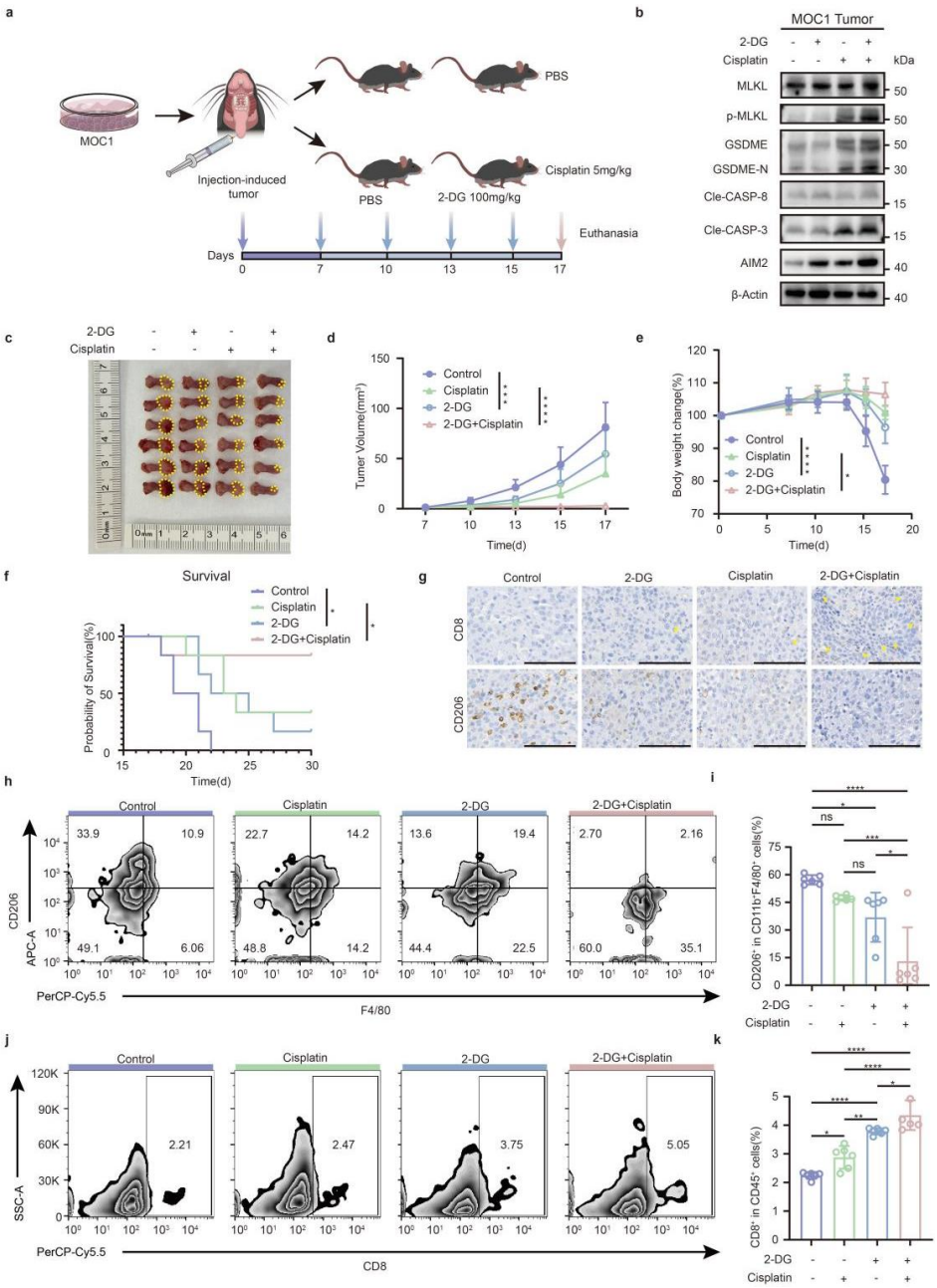

Fig. 5. Combined 2-DG and cisplatin treatment enhances therapeutic efficacy *in vivo*

(a) Experimental design of MOC1 tumor inoculation followed by i.p. treatments (PBS, 2-DG, cisplatin, or combination) on days 7, 10, 13 and 15. **(b)** Western blot analysis of PANoptosis markers (Cleaved Caspase-3/8, p-MLKL, MLKL, GSDME, GSDME-N, AIM2) in tumor tissues. **(c)** Macroscopic tongue tumors in C57BL/6 mice bearing MOC1 cells after treatment with PBS, 2-DG (100 mg/kg), cisplatin (5 mg/kg), or combination. **(d, e)** Tumor growth (**d**) and body weight (**e**) curves. **(f)** Survival analysis of each group. **(g)** Representative IHC

staining of $CD8^+$ T cells and M2 macrophages in tumors (scale bar: 100 μm). **(h-k)** Flow cytometry analysis **(h)** and quantification **(i)** of M2 macrophages; Flow cytometry analysis **(j)** and quantification **(k)** of $CD8^+$ T cells. The data presented in this figure are expressed as mean ± *S.D.*; sample size, $n = 6$, biological replicates; Statistical analyses: *t*-test and two-way ANOVA. $^*P < 0.05$, $^{**}P < 0.01$; $^{***}P < 0.001$, $^{****}P < 0.0001$.

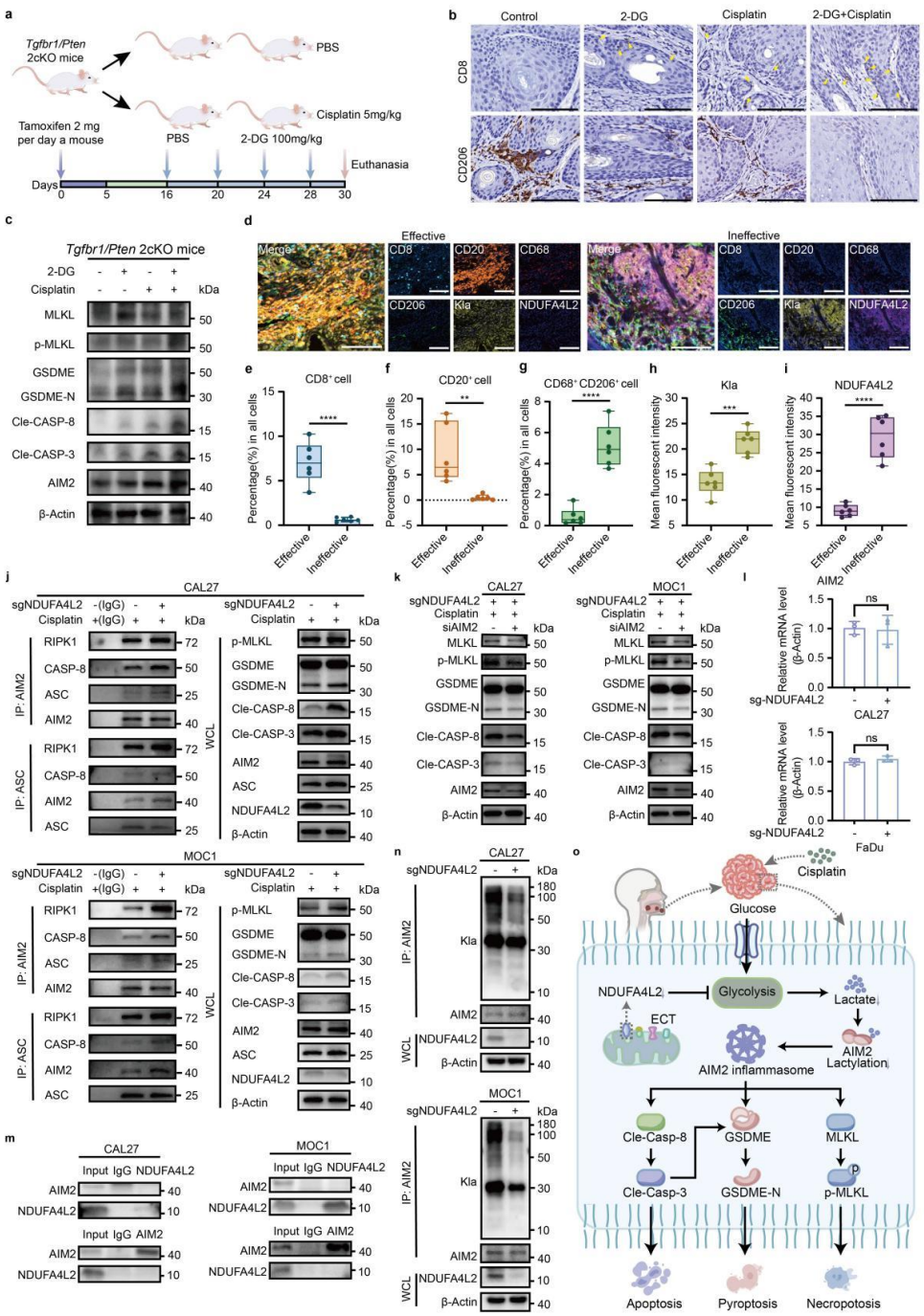

Fig. 6. NDUFA4L2 knockout regulates PANoptosis by inhibiting AIM2 lactylation

(a) Experimental timeline for *Tgfbr1/Pten* 2cKO mice: Tamoxifen induction (2 mg/day ×5 days) followed by i.p. treatments (PBS, 2-DG, cisplatin, or combination) on days 16, 20, 24 and 28. **(b)** Representative IHC staining

of $CD8^+$ T cells and M2 macrophages in *Tgfbr1/Pten* 2cKO tumors across treatment groups (scale bar: 100 μm; $n = 3$, biological replicates). **(c)**Western blot analysis of PANoptosis markers (Cleaved Caspase-3/8, p-MLKL, MLKL, GSDME, GSDME-N, AIM2) in tumor tissues. **(d)** mIHC showing expression of CD8 (cyan), CD20 (orange), CD68 (red), CD206 (green), Kla (yellow-green), and NDUFA4L2 (magenta) in chemotherapy-sensitive vs resistant patient tumors. **(e-i)** Quantitative Analysis of $CD8^+$, $CD20^+$, $CD68^+CD206^+$ Cell Proportions and NDUFA4L2/Kla MFI in mIHC (scale bar: 100 μm; $n = 6$, biological replicates; $^*P < 0.05$, $^{**}P < 0.01$; $^{***}P < 0.001$, $^{****}P < 0.0001$.). **(j)** Co-IP assays demonstrating the AIM2-ASC interaction and their binding to CASPASE-8/RIPK1 in cisplatin-treated wild-type and NDUFA4L2-KO CAL27 and MOC1 cells. Western blot analysis of PANoptosis markers in WCL. **(k)** Western blot analysis of PANoptosis markers (cle-caspase-3/8, p-MLKL, GSDME-N) expression following cisplatin treatment in CAL27 cells and MOC1 cells with NDUFA4L2 knockout and AIM2 knockdown**. (l)** Relative mRNA levels of AIM2 in wild-type vs NDUFA4L2-KO CAL27 and FaDu cells (mean ± *S.D.*; $n = 3$, biological replicates; ns: $P > 0.05$). **(m)** Co-IP demonstrating the interaction between NDUFA4L2 and AIM2 in CAL27 and MOC1 cells (upper panel: IP with anti-NDUFA4L2, blot for AIM2; lower panel: IP with anti-AIM2, blot for NDUFA4L2). **(n)** IP and Western blot analysis of AIM2 lactylation levels in control vs NDUFA4L2-KO cells. **(o)** Schematic diagram of the proposed model in this study: NDUFA4L2-mediated glycolysis inhibits AIM2-dependent PANoptosis, conferring cisplatin resistance.

Table 1. Patient data involved in this study

Sample	Sex	Age	TNM Classification	Stage	Chemotherapy	Sensitivity
Patient1	Male	35	Tis	0	No	-
Patient2	Female	66	T1N0M0	I	No	-
Patient3	Male	36	T2N0M0	II	No	-
Patient4	Female	54	T3N0M0	III	No	-
Patient5	Male	70	T3N2M0	IV	No	-
Patient6	Male	87	T2N1M0	III	No	-
Patient7	Female	57	T3N0M0	III	No	-
Patient8	Female	72	T2N0M0	II	No	-
Patient9	Female	73	T2N0M0	II	No	-
Patient10	Male	65	T3N3M0	IV	No	-
Patient11	Male	52	T3N2M0	IV	YES	Se
Patient12	Female	65	T2N0M0	II	YES	Se
Patient13	Male	66	T3N1M0	III	YES	Se
Patient14	Female	77	T4N1M0	IV	YES	Se
Patient15	Male	66	T4N0M0	IV	YES	Se
Patient16	Male	71	T2N3M0	IV	YES	Se
Patient17	Male	58	T3N0M0	III	YES	NS
Patient18	Male	58	T3N1M0	III	YES	NS
Patient19	Male	70	T3N3M0	IV	YES	NS

Patient20	Female	66	T4N0M0	IV	YES	NS
Patient21	Female	72	T2N3M0	IV	YES	NS
Patient22	Male	70	T4N0M0	IV	YES	NS

TNM classification and tumor staging are determined by the Union for International Cancer Control (UICC); NS insensitive, SE sensitive.

Table 2. Primary antibodies

Antibodies	Sourse	Identifier
anti-caspase-3/cleaved-caspase-3	Proteintech	Cat No.19677-1-AP
anti-caspase-8/cleaved-caspase-8	Proteintech	Cat No.13423-1-AP
anti-MLKL	Proteintech	Cat No.66675-1-Ig
anti-p-MLKL	Affinity	Cat. #AF7420
anti-GSDME	Abcam	Cat# ab215191
anti-AIM2	Cell Signaling Technology	Cat# 53491(M); Cat# 12948(H)
anti-NDUFA4L2	Proteintech	Cat No.16480-1-AP
anti-CD8α	Cell Signaling Technology	Cat# 98941(M); Cat# 85336(H)
anti-CD206	Cell Signaling Technology	Cat# 24595
anti-CD68	Cell Signaling Technology	Cat# 76437
anti-CD20	Sino Biological	Cat# IHC012
anti-L-Lactyl Lysine	PTM BIO	Cat# PTM-1401
anti-ASC	ABclonal	Cat# A22046
anti-RIPK1	ABclonal	Cat# A7414
anti-RNLRP3	ABclonal	Cat# A5652
anti-ZBP1	Cell Signaling Technology	Cat# 33402(M); Cat# 60968(H)
anti-β-actin	Proteintech	Cat No.66009-1-Ig